Journal of The Electrochemical Society, **147** (11) 4196-4202 (2000)
S0013-4651(00)03-078-0 CCC: $7.00

Structural and Electrical Characterization of a Novel Mixed Conductor: CeO_2-Sm_2O_3-ZrO_2 Solid Solution

W. Huang,[a] P. Shuk,[a,d,*] M. Greenblatt,[a,z] M. Croft,[b] F. Chen,[c,] and M. Liu[c,*]**

[a]*Department of Chemistry and* [b]*Department of Physics, Rutgers, the State University of New Jersey, Piscataway, New Jersey 08854, USA*
[c]*School of Materials Science and Engineering, Georgia Institute of Technology, Atlanta, Georgia 303320, USA*

$(Ce_{0.83}Sm_{0.17})_{1-x}Zr_xO_{2-\delta}$ (x = 0 to 0.50) solid solutions were synthesized for the first time by the hydrothermal method. The electrical properties of the solid solutions have been studied in air and under reducing conditions. Solid solutions with the fluorite structure were formed in all of the studied range of ZrO_2 substitution after calcination at 1500°C. With increasing ZrO_2 substitution up to 30 mol %, the electronic conductivity increases under a reducing atmosphere. The $(Ce_{0.83}Sm_{0.17})_{0.7}Zr_{0.3}O_{2-\delta}$ solid solution has good mixed electronic and ionic conductivity; the total conductivity is 0.42 S/cm at $p_{O_2} = 5.7 \times 10^{-21}$ atm and 700°C with an estimated ionic conductivity of *ca*. 10^{-2} S/cm.

Manuscript submitted March 17, 2000; revised manuscript received July 7, 2000.

Solid electrolytes are key components of solid-state electrochemical devices, which are increasingly important for applications in energy conversion, chemical processing, sensing, and combustion control.[1-3] Solid electrolytes based on CeO_2^4 also have potential applications as structural and electronic promoters of heterogeneous catalytic reactions and oxygen membranes.[4-8]

In recent years the CeO_2-ZrO_2 system has been investigated, mainly in the context of a "three-way catalyst" technology for the treatment of automobile exhausts.[9-13] It has been reported that the reducibility of ceria is greatly enhanced when it is mixed with zirconia to form a solid solution.[9-13] These results suggest that CeO_2-ZrO_2 might be an excellent mixed conductor (exhibiting both ionic and electronic conductivity). It is the numerous applications of mixed conductors as oxygen separation membranes, partial oxidation catalysts, and fuel-cell electrodes that motivated us to investigate the CeO_2-ZrO_2 solid solution as a potential mixed conductor. Recently we have shown that solid solutions of $Ce_{1-x}Sm_xO_{2-x/2}$ and $Ce_xCa_xO_{2-x}$ can be hydrothermally prepared in a wide substitution range of Sm or Ca.[14] Our systematic studies showed maximum ionic conductivity for the $Ce_{0.83}Sm_{0.17}O_{2-\delta}$ composition. In order to achieve appreciable ionic conductivity in the mixed conductor, we have investigated the substitution of $Ce_{0.83}Sm_{0.17}O_{2-\delta}$ with 0 to 50 mol % ZrO_2, *i.e.*, $(Ce_{0.83}Sm_{0.17})_{1-x}Zr_xO_{2-\delta}$ (x = 0 to 0.5) solid solutions. In this paper we report the results of these studies.

Experimental

Synthesis.—Solid solutions of $(Ce_{0.83}Sm_{0.17})_{1-x}Zr_xO_{2-\delta}$ (x = 0 to 0.50) were synthesized by the hydrothermal method as previously reported for the Tb, Sm, and Ca doped ceria solid electrolytes.[7,14] The appropriate quantities of cerium(III) nitrate hexahydrate [$Ce(NO_3)_3 \cdot 6H_2O$, 99.9% Aldrich], samarium(III) nitrate hexahydrate [$Sm(NO_3)_3 \cdot 6H_2O$, 99.9% Aldrich], and zirconium dichloride oxide hexahydrate ($ZrOCl_2 \cdot 6H_2O$, 99.9% Aldrich) were dissolved separately in water, mixed and coprecipitated with ammonium hydroxide at pH 10. The precipitated gels were sealed into Teflon-lined steel autoclaves and hydrothermally treated at 260°C for several hours. The autoclaves were quenched, and the crystallized powder of $(Ce_{0.83}Sm_{0.17})_{1-x}Zr_xO_{2-\delta}$ (x = 0 to 0.50) solid solutions were repeatedly washed with deionized water and dried in air at room temperature.

X-ray diffraction.—The powder X-ray diffraction patterns (XRD) of the ultrafine powder samples were obtained with a Scintag PAD V diffractometer equipped with monochromatized Cu Kα radiation at a 2θ scan of 0.5°/min. Cell parameters were calculated by fitting the observed reflections with a least-squares program.

XAS measurements.—The X-ray absorption spectroscopy (XAS) measurements were made in the electron yield and fluorescence modes[15-17] on beam line X-19A at the Brookhaven National Synchrotron Light Source with double crystal [Si(111)] and monochromater. All spectra were normalized to unity step in the absorption coefficient from well below to well above the edge.

Electrical conductivity measurement.—The powder samples were pelletized and sintered at 1500°C for 24 h with a programmed heating and cooling rate of 5°C/min. The sintered samples were over 95% of the theoretical density in all cases, as determined by pycnometry.

The ionic conductivity of the materials was measured on a sintered ceramic pellet. Silver paste was painted onto two faces of the pellets, using GC Electronics paste. The sample was then dried and fired at 700°C. The ionic conductivity measurements were performed by the complex-impedance method at frequencies ranging from 0.1 Hz to 20 kHz (Solartron 1280 frequency response analyzer) on isothermal plateaus 1 h long, in air on heating and cooling every 25 to 50°C up to 800°C.

The electrical conductivity of ceria samples was measured as a function of oxygen partial pressure, p_{O_2}, and temperature with a four-probe dc technique. A mixture of O_2, N_2, and H_2 gases passed through a water separator, set at 25 to 85°C, was used to fix different oxygen partial pressures determined from the equilibrium of the chemical reactions of the gases. The oxygen partial pressure in the gas mixture was measured by a solid-electrolyte oxygen sensor before and after the gasses passed through the closed ceramic cell where the ceria solid electrolyte sample was placed for the conductivity measurements. The samples were allowed to equilibrate at the set p_{O_2} atmospheres for 24 h before the measurement was taken.

Electrode polarization measurement.—For the electrode polarization measurements, the ceria samples were prepressed uniaxially, then isostatically under 500 MPa. The green densities were about 55 to 58%. The green pellets were sintered at 1400°C for 1 h with a programmed heating and cooling rate of 5°C/min. The sintered samples were over 98% of the theoretical density in all cases. Platinum electrodes were attached with a commercial electrode process. First a thin Pt film was sprayed on the pellet surface and then sintered at 1200°C; finally the Engelhard Pt paste was used to optimize the electrode properties. The sample was dried in air and fired at 900°C. The impedance measurements were performed with an impedance analyzer SI-1260 (Solartron Instruments) over 0.01 Hz to 1 MHz frequency range on isothermal plateaus 1 h long, in air on heating every 50°C up to 650°C. The inductive error associated with various components of the measurement circuit was evaluated by carrying

* Electrochemical Society Active Member.
** Electrochemical Society Student Member.
[d] Present address: Rosemount Analytical, Inc., Orrville, OH 44667-0901, USA.
[z] E-mail: martha@rutchem.rutgers.edu

S0013-4651(00)03-078-0 CCC: $7.00

out measurements in the rig on reference resistances in place of samples. All the measurements were corrected accordingly. The curve fitting was done with "Zview 2.1b" with different equivalent circuits. The solid-electrolyte conductivities as well as polarization resistances of the applied electrodes were determined directly from the impedance spectra.

Ionic and electronic transference numbers measurement.—The ionic and electronic transference numbers were determined with a combination of impedance spectroscopy, open-circuit voltage measurement, and oxygen gas permeation measurements. Figure 1 shows a schematic arrangement for these measurements. Cells with Pt electrodes were attached to an alumina tube using a glass seal.[18] The glasses were fired *in situ*, and the heating and cooling rates were carefully controlled to avoid cracking of the glass seal. The furnace was heated at 7°C/min to 820°C, held at that temperature for 10 min to soften the glass, and then cooled at 3°C/min to the desired temperature for testing. Impedance spectra, open-circuit potentials, and oxygen permeation rates were measured under identical conditions in an oxygen concentration cell

$$\text{Air, Pt} \mid (Ce_{0.83}Sm_{0.17})_{1-x}Zr_xO_{2-\delta} \mid \text{Pt, Ar (or } H_2) \qquad [1]$$

The oxygen concentration of the incoming and outgoing gas was monitored with an yttria-stabilized zirconia (YSZ) oxygen sensor. A computerized impedance-analysis system, consisting of a frequency response analyzer (Solartron 1255) and an electrochemical interface (Solartron 1286), was used to measure the impedance of the oxygen concentration cells in the frequency range from 1 mHz to 10 MHz at temperatures ranging from 500 to 750°C.

Measurement of defect concentration.—The electrical conductivity of doped ceria under reducing atmospheres is different from that under high oxygen activities because of the reduction of cerium cations from Ce^{4+} to Ce^{3+}. Such reduction must at the same time give rise to a weight loss of the samples due to oxygen loss, which can be measured by thermogravimetric techniques.

The $(Ce_{0.83}Sm_{0.17})_{0.7}Zr_{0.3}O_{2-\delta}$ sample was first calcined at a high temperature, 1500°C. A thermogravimetric analyzer TGA (TA Instruments, Inc., model 2050) was used to examine the weight change under reducing atmospheres. The partial pressure of oxygen was controlled by a N_2/H_2 flow and measured by a YSZ oxygen sensor placed at the outlet of the balance. Measurements were carried out isothermally at a fixed flow rate of gases.

The composition of the solid solution in air is taken as a stoichiometric reference and may be explicitly written as $(Ce_{0.83}Sm_{0.17})_{0.7}Zr_{0.3}O_{1.94}$. Under reducing atmospheres, the composition of the solid solutions departs from the "stoichiometric" composition by a value δ, according to $Ce_{(0.83\times7)-2\delta}Sm_{(0.17\times0.7)}Zr_{0.3}O_{1.94-\delta}$. The deviation from stoichiometry δ can be obtained from[19,23]

$$(Ce_{0.83}Sm_{0.17})_{0.7}Zr_{0.3}O_{1.94} \rightarrow Ce^{4+}_{(0.83\times0.7)-2\delta}Ce^{3+}_{2\delta}Sm_{0.17\times0.7}Zr_{0.3}O_{1.94-\delta} + \frac{\delta}{2}O_2 \qquad [2]$$

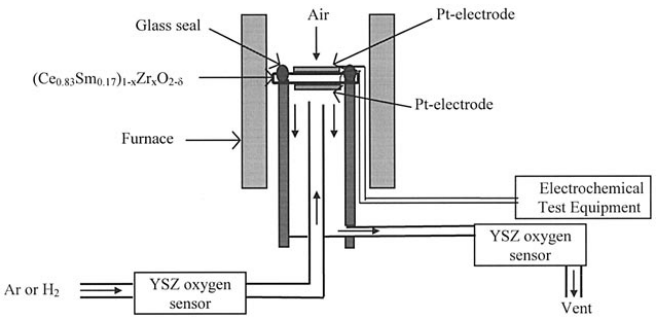

Figure 1. A schematic diagram showing the experimental arrangement for gas permeation, open-circuit potential, and impedance measurements.

$$\delta = \frac{2(m_{air} - m)M_{sample}}{m_{air}M_{O_2}} \qquad [3]$$

where m_{air} and m represent the mass of the sample in air and reducing atmospheres, respectively, M_{sample} and M_{O_2} are the molar mass of the sample and oxygen molecule, respectively.

Results and Discussion

Phase composition.—X-ray diffraction (XRD) analysis (Fig. 2) indicates that the $(Ce_{0.83}Sm_{0.17})_{1-x}Zr_xO_{2-\delta}$ solid solutions prepared by the hydrothermal method at 260°C for $x = 0.0$ to 0.10 form with the cubic fluorite structure, while for $x = 0.2$ to 0.50 a zirconia tetragonal impurity phase is present along with the cubic fluorite phase. When the hydrothermal processing temperature is increased to 310°C, the XRD shows the zirconia tetragonal impurity phase only for $x = 0.5$. However, when the hydrothermally prepared solid solutions ($x = 0.2$ to 0.5; 260°C) are calcined at 1500°C for 12 h, the XRD (Fig. 3) shows no evidence of tetragonal zirconia. Figure 4 shows the phase evolution of $(Ce_{0.83}Sm_{0.17})_{0.5}Zr_{0.5}O_{2-\delta}$ in the range from 260 to 1300°C; the zirconia tetragonal impurity phase disappears, and the resulting diffraction peaks of the ceria fluorite phase are shifted to higher 2θ as the temperature is increased. Rietveld refinement (Fig. 5) also confirms that the resulting phase is a fluorite structure (space group *Fm*3*m*) where Ce, Sm, and Zr are statistically distributed in the special position 4(a).

The unit-cell parameter for $(Ce_{0.83}Sm_{0.17})_{1-x}Zr_xO_{2-\delta}$ ($x = 0$ to 0.50) solid solution (inset in Fig. 3) calcined at 1500°C decreases linearly with the zirconia content according to Vegard's law and as expected from effective ionic radii ($r_{Ce^{4+}} = 0.1110$ nm; $r_{Sm^{3+}} = 0.1219$ nm; $r_{Zr^{4+}} = 0.0980$ nm[20]) considerations.

Zr-$L_{2,3}$ spectral changes between the cubic and tetragonal structures.—The WL ("white line") features at the L_3 (L_2) edges of 4d transition metal compounds are related to $2p_{3/2}$ ($2p_{1/2}$) to $4d_{5/2}$-$4d_{3/2}$ and ($4d_{3/2}$) phototransitions. Consequently these WL features yield direct information on the occupancy and energy distribution of the important final 4d states (with the understanding that the final state 2p hole and multiplet interactions can also play a complicating role). The Zr atoms in $(Ce_{0.83}Sm_{0.17})_{1-x}Zr_xO_{2-\delta}$, $0 \le x \le 0.5$ are in an eight-fold cubic environment for which the four-fold degenerate e_g

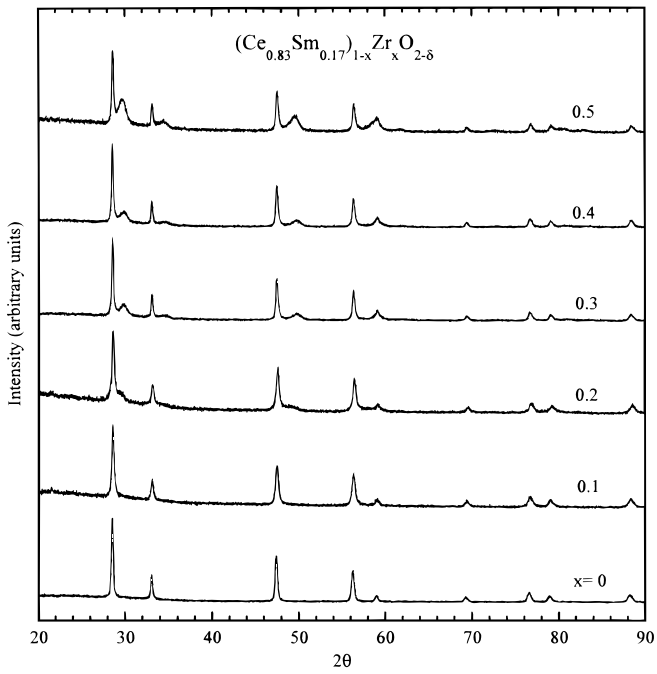

Figure 2. XRD patterns of the $(Ce_{0.83}Sm_{0.17})_{1-x}Zr_xO_{2-\delta}$ solid solutions ($x = 0.0$ to 0.50) prepared by hydrothermal methods at 260°C.

S0013-4651(00)03-078-0 CCC: $7.00

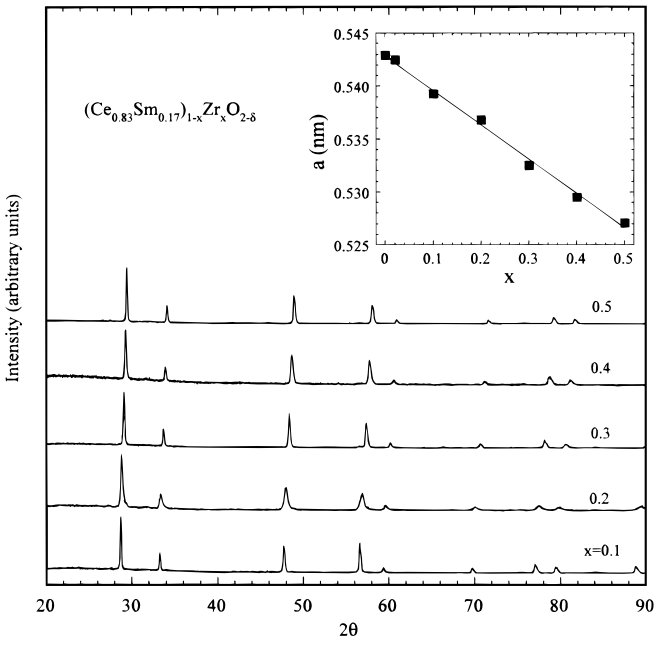

Figure 3. XRD patterns of the $(Ce_{0.83}Sm_{0.17})_{1-x}Zr_xO_{2-\delta}$ solid solutions (x = 0.1 to 0.50) prepared by hydrothermal methods at 260°C and calcined at 1500°C. Inset: variation of the lattice parameters as a function of x for $(Ce_{0.83}Sm_{0.17})_{1-x}Zr_xO_{2-\delta}$ solid solutions (x = 0.0 to 0.50) prepared by hydrothermal methods at 260°C and calcined at 1500°C.

orbitals lie at an energy Δ below the six-fold t_{2g} orbitals. The Zr-$L_{2,3}$ spectra for $(Ce_{0.83}Sm_{0.17})_{0.5}Zr_{0.5}O_{2-\delta}$ in Fig. 6 manifest a clearly bimodal structure with the less (more) intense, lower (higher) energy A feature (C feature) involving the e_g (t_{2g}) final states. The magnitude of the crystalline electric field (CEF) splitting is about Δ = 2.3 eV from the A-C feature splitting. Orlando *et al.*[21] noted the clear e_g-t_{2g} splitting (with an intervening gap) in their *ab initio* Hartree-Fock calculation of the d-projected density states (DOS) for cubic ZrO_2. Their projected DOS figure exhibits a roughly 2 eV splitting between the band centroids which, without a full photoabsorption calculation, is in adequate agreement with the Zr-$L_{2,3}$ results presented here.

The Zr-$L_{2,3}$ spectra for tetragonally distorted fluorite $ZrO_{2-\delta}$ in Fig. 6 manifest a similar two peak A-C structure. The additional spectral intensity of the A and C peaks of $ZrO_{2-\delta}$ is dramatic in comparison to $(Ce_{0.83}Sm_{0.17})_{0.5}Zr_{0.5}O_{2-\delta}$ spectrum. Moreover, in the XAS of $ZrO_{2-\delta}$ an additional unresolved intermediate B feature (or features) is also present. The higher intensity of the B feature in the L_3 spectrum is related to spin orbit and multiplet effects. It is well known that when the cubic O_h symmetry is lowered to tetragonal D_{4h} symmetry, the (x^2-y^2) and (z^2) of the e_g orbitals split in energy and the (t_{2g}) orbitals split into [(xz), (yz)] and [xy] energy states. Thus the intermediate energy states of the B feature in the Zr-$L_{2,3}$ spectra of $ZrO_{2-\delta}$ in Fig. 6 are consistent with these lower symmetry splittings. Indeed the d projected DOS for tetragonal-$ZrO_{2-\delta}$, of Orlando *et al.*[21] manifests a dramatic filling-in of intermediate energy states in the e_g–t_{2g} gap seen for cubic $ZrO_{2-\delta}$. Thus these *ab initio* calculations support the character of the observed Zr-$L_{2,3}$ spectral changes between the cubic and tetragonal fluorite-based structures.

Ionic conductivity in air.—The composition and temperature dependences of ionic conductivity of $(Ce_{0.83}Sm_{0.17})_{1-x}Zr_xO_{2-\delta}$ solid solutions (x = 0.0 to 0.50) in air are shown in Fig. 7. It can be seen that in the lower ZrO_2 substitution range (x = 0.0 to 0.30), the ionic conductivity decreases with increasing ZrO_2, whereas $(Ce_{0.83}Sm_{0.17})_{0.5}Zr_{0.5}O_{2-\delta}$ and $(Ce_{0.83}Sm_{0.17})_{0.6}Zr_{0.4}O_{2-\delta}$ exhibit higher ionic conductivity than $(Ce_{0.83}Sm_{0.17})_{0.7}Zr_{0.3}O_{2-\delta}$. The inset in Fig. 7 shows that the apparent activation energy (E_a) tends to increase with ZrO_2 content up to x = 0.2, and for x > 0.2, E_a is constant within the experimental error (±0.05 eV).

The incorporation of $SmO_{1.5}$ in the CeO_2 or ZrO_2 host structure can be described by the following equation

$$2SmO_{1.5} \rightarrow 2Sm'_{Ce/Zr} + 3\,O_o^x + V_O^{\cdot\cdot} \qquad [4]$$

Notice that Kröger–Vink notation[22] is used in this equation in which $V_O^{\cdot\cdot}$ represents an oxygen vacancy, $Sm'_{Ce/Zr}$ is a Sm^{3+} on a Ce^{4+} or Zr^{4+} lattice site, and O_o^x is a normal oxygen lattice site. It is expected that in the lower ZrO_2 substitution range (x = 0.0 to 0.30), the [Sm^{3+}] will decrease in the cubic fluorite host structure. Since *ca.* 17 mol % Sm^{3+} is the optimal concentration for $Ce_{1-x}Sm_xO_{2-\delta}$ to achieve maximum ionic conductivity, decreasing [Sm^{3+}] in

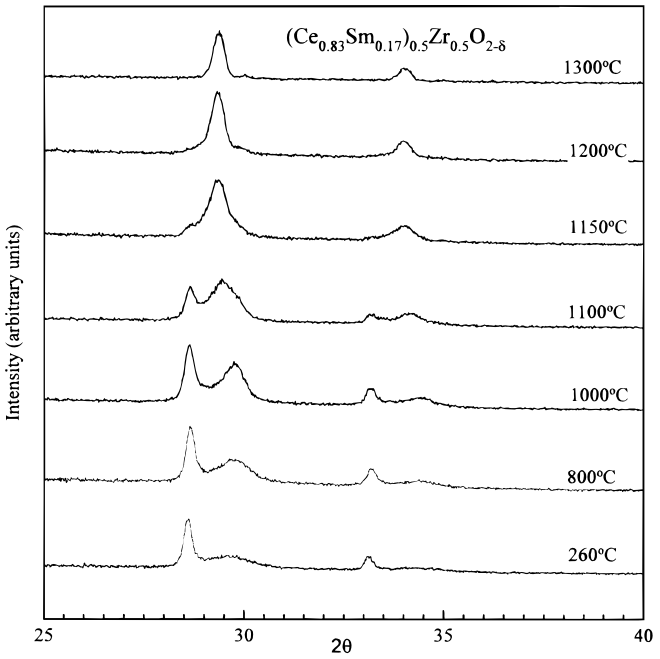

Figure 4. Phase evolution of $(Ce_{0.83}Sm_{0.17})_{0.5}Zr_{0.5}O_{2-\delta}$ solid solution in the temperature range 260 to 1300°C.

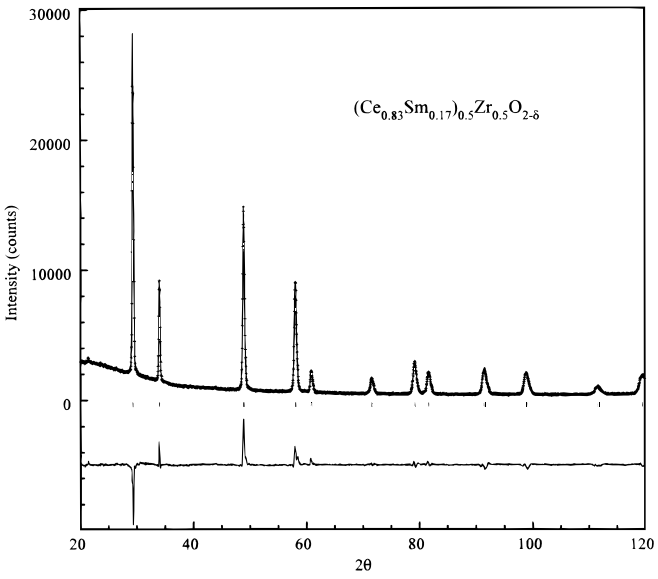

Figure 5. Observed (+), calculated (solid line), and difference XRD profiles of $(Ce_{0.83}Sm_{0.17})_{0.5}Zr_{0.5}O_{2-\delta}$ (after calcined at 1400°C for 24 h). Reflection positions are represented by tic marks. Space group: $Fm3m$; a = 0.52721(4) nm; atomic positions: Ce, Sm, Zr in 4(a); O in 8(c) (Wyckoff notation); R_p = 5.7%; R_{wp} = 8.0%.

S0013-4651(00)03-078-0 CCC: $7.00

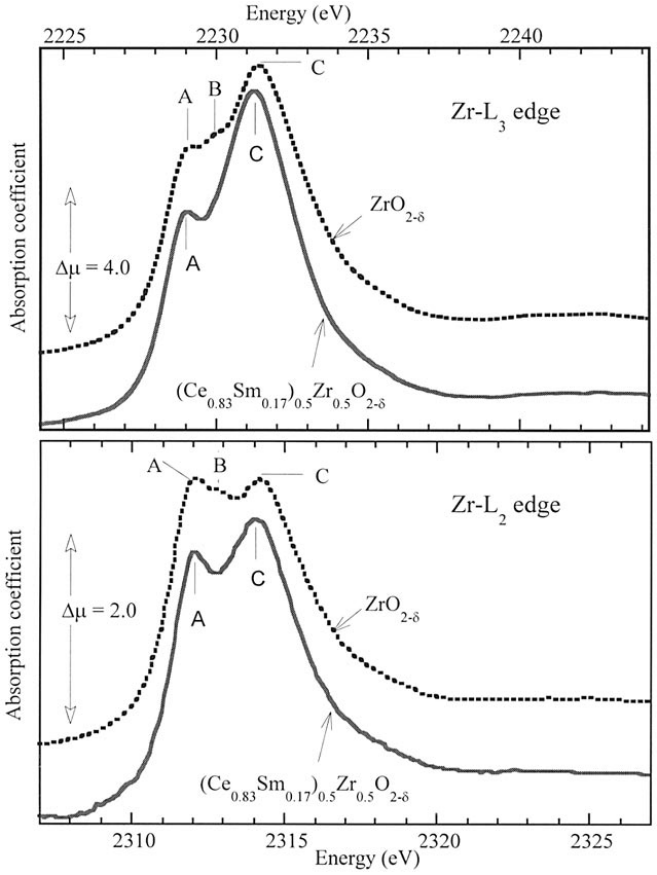

Figure 6. The Zr-L_3 and L_2 spectra for cubic-fluorite $(Ce_{0.83}Sm_{0.17})_{0.5}Zr_{0.5}O_{2-\delta}$ and for ZrO_2 with a tetragonally distorted fluorite structure. Note the A and C features of the cubic material that are associated with the four-fold e_g and six-folds t_{2g} orbitals, respectively, with the CEF splitting, Δ, being *ca*. 2.3 eV.

$(Ce_{0.83}Sm_{0.17})_{1-x}Zr_xO_{2-\delta}$ will lead to lower $[V_O^{\cdot\cdot}]$ and thus the observed lower ionic conductivity as x increases up to 0.30 (Fig. 7).

Electrical conductivity in the low oxygen partial pressure (p_{O_2}) region.—The electrical conductivity of the $(Ce_{0.83}Sm_{0.17})_{1-x}Zr_xO_{2-\delta}$ solid solution for $x = 0$, 0.02, 0.08 0.2, and 0.3 in the low p_{O_2} region is shown in Fig. 8. The electrical conductivity tends to increase with decreasing p_{O_2}. The increased electrical conductivity in the low p_{O_2} region can be attributed to the partial reduction of the Ce^{4+} to generate electronic charge carriers according to the reaction

$$2Ce_{Ce}^{x} + O_O = 2Ce_{Ce}^{'} + V_O^{\cdot\cdot} + \frac{1}{2}O_2 \qquad [5]$$

where Ce_{Ce}^{x} is a Ce^{4+} on a Ce^{4+} lattice site and $Ce_{Ce}^{'}$ is a Ce^{3+} on a Ce^{4+} lattice. For a stoichiometric reaction, it can be assumed that $[Ce_{Ce}^{'}] = 2[V_O^{\cdot\cdot}]$, where $[Ce_{Ce}^{'}]$ and $[V_O^{\cdot\cdot}]$ are concentrations of $Ce_{Ce}^{'}$ and $V_O^{\cdot\cdot}$, respectively. Thus

$$[Ce_{Ce}^{'}] = K^{1/2}[Ce_{Ce}^{x}][O_O^{x}]^{1/2}[V_O^{\cdot\cdot}]^{-1/2}p_{O_2}^{-1/4} \qquad [6]$$

where K is the equilibrium constant for Eq. 5.

If the concentration of intrinsic electrons and holes as well as oxygen interstitials in the samples is negligible, the electroneutrality condition can be described as

$$2[V_O^{\cdot\cdot}] = [Ce_{Ce}^{'}] + [Sm_{Ce/Zr}^{'}] \qquad [7]$$

It follows then that

$$[Ce_{Ce}^{'}] = (2K)^{1/2}[Ce_{Ce}^{x}][O_O^{x}]^{1/2}([Ce_{Ce}^{'}] + [Sm_{Ce/Zr}^{'}])^{-1/2}p_{O_2}^{-1/4} \qquad [8]$$

Assume $[O_O^{x}]$ and $[Ce_{Ce}^{x}]$ are constants; Eq. 8 can be simplified as

$$[Ce_{Ce}^{'}] = K'([Ce_{Ce}^{'}] + [Sm_{Ce/Zr}^{'}])^{-1/2}p_{O_2}^{-1/4} \qquad [9]$$

where $K' = (2K)^{1/2}\,[Ce_{Ce}^{x}][O_O^{x}]^{1/2}$.

It follows from Eq. 9 that if $[Ce_{Ce}^{'}] << [Sm_{Ce/Zr}^{'}]$ (most likely in the lower ZrO_2 content samples and at high oxygen partial pressures), $[Ce_{Ce}^{'}] \propto p_{O_2}^{-1/4}$, whereas if $[Ce_{Ce}^{'}] \approx [Sm_{Ce/Zr}^{'}]$ at very low p_{O_2}, $[Ce_{Ce}^{'}] \propto p_{O_2}^{-1/6}$.

If electron hopping from Ce^{3+} to Ce^{4+} is the main charge-carrier process, and the electron mobility is constant, the n-type electronic conductivity is proportional to $[Ce_{Ce}^{'}]$ and should have the same oxygen-activity dependence as $[Ce_{Ce}^{'}]$, *i.e.*, the n-type electronic conductivity is dependent upon the oxygen pressure to the power of *ca*. −1/6 to −1/4.

As seen in Fig. 8, the observed slopes for the least-square best fitted straight lines (log σ *vs.* log p_{O_2}) for $(Ce_{0.83}Sm_{0.17})_{1-x}Zr_xO_{2-\delta}$ solid solutions with $x = 0$, 0.02, 0.08, 0.2, and 0.3 are −0.17, −0.22, −0.24, −0.14, and −0.12, respectively. The slopes of $x = 0$, 0.02, and 0.08 are within the range −1/6 to −1/4, indicating n-type electronic conductivity. In the case of $(Ce_{0.83}Sm_{0.17})_{0.8}Zr_{0.2}O_{2-\delta}$ and $(Ce_{0.83}Sm_{0.17})_{0.7}Zr_{0.3}O_{2-\delta}$, the absolute value of the slope is lower than 1/6. This might be due to the increase of the ionic conductivity under reducing atmospheres, as the reduction of Ce^{4+} leads to an increase of the oxygen-vacancy concentration. Since the oxygen-vacancy concentration of $(Ce_{0.83}Sm_{0.17})_{0.7}Zr_{0.3}O_{2-\delta}$ in air is lower than that in $Ce_{0.83}Sm_{0.17}O_{2-\delta}$, an increased oxygen-vacancy concentration should give rise to an increase of ionic conductivity. In the following discussion, we use an established procedure described previously by Mogensen *et al.*,[23] specifically, in the range of p_{O_2} from 5.0×10^{-18} to 4.8×10^{-22} atm, thermogravimetric measurements indicate that in $Ce^{4+}_{(0.83\times0.7)-2\delta}Ce^{3+}_{2\delta}Sm_{(0.17\times0.7)}Zr_{0.3}O_{1.94-\delta}$ δ changes from 0.0274 to 0.0536 (Table I). The total oxygen-vacancy concentration of $Ce^{4+}_{(0.83\times0.7)-2\delta}Ce^{3+}_{2\delta}Sm_{(0.17\times0.7)}Zr_{0.3}O_{1.94-\delta}$ under these conditions

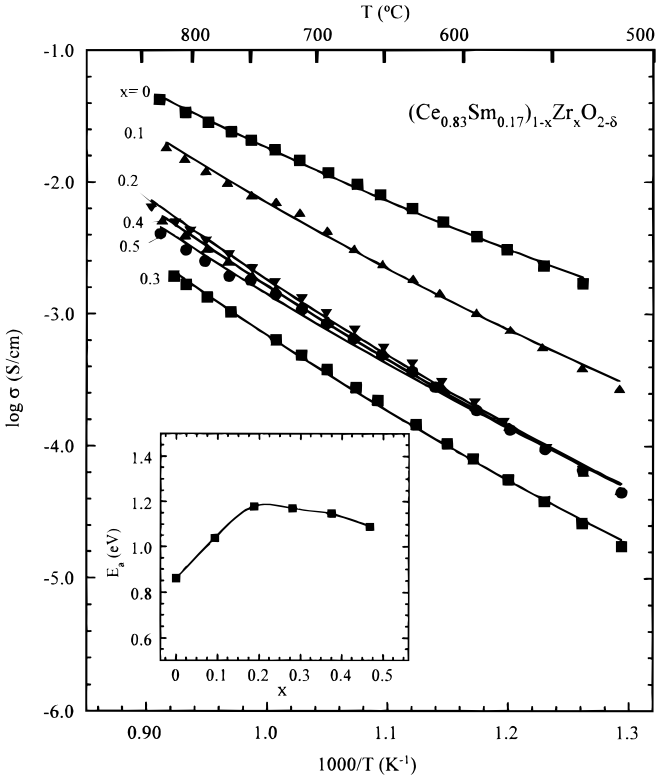

Figure 7. Temperature dependence of the ionic conductivity of the $(Ce_{0.83}Sm_{0.17})_{1-x}Zr_xO_{2-\delta}$ solid solutions ($x = 0.0$ to 0.50). Inset: composition dependence of activation energy of the $(Ce_{0.83}Sm_{0.17})_{1-x}Zr_xO_{2-\delta}$ solid solutions ($x = 0.0$ to 0.50).

S0013-4651(00)03-078-0 CCC: $7.00

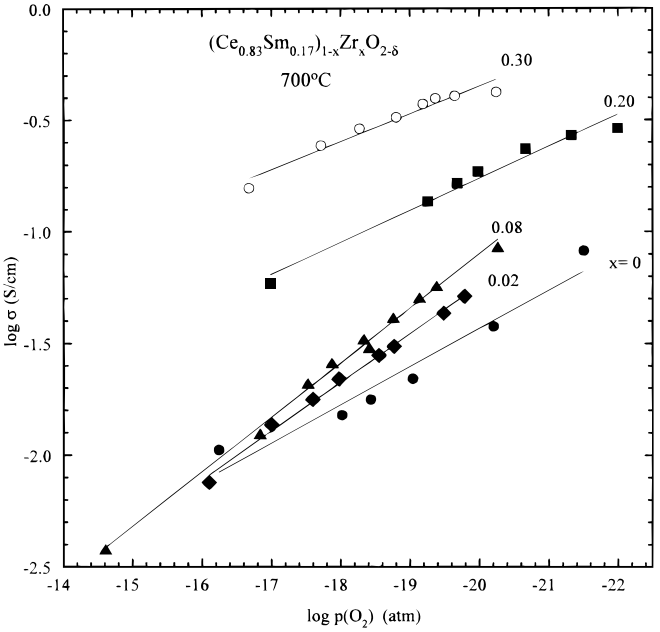

Figure 8. Total electrical conductivity of the $(Ce_{0.83}Sm_{0.17})_{1-x}Zr_xO_{2-\delta}$ solid solutions (x = 0.0 to 0.50) under reducing atmospheres and at 700°C.

($p_{O_2} = 5 \times 10^{-18}$ to 5×10^{-22} atm) is the same as the oxygen-vacancy concentration generated by doping pure ceria with 17.4 to 22.8 mol % Sm^{3+} in air. Although direct measurement of ionic conductivity has not been possible under reducing atmospheres, it is reasonable to estimate that the ionic conductivity of $(Ce_{0.83}Sm_{0.17})_{0.7}Zr_{0.3}O_{2-\delta}$ under reducing atmospheres ($p_{O_2} = 5 \times 10^{-18}$ atm) is *ca*. 0.01 S/cm, as observed in the sample $Ce_{0.8}Sm_{0.2}O_{2-\delta}$ at 700°C in air.

Figure 8 also shows that at a fixed p_{O_2} the larger the ZrO_2 content, the higher the electrical conductivity. The total electrical conductivity of $(Ce_{0.83}Sm_{0.17})_{0.7}Zr_{0.3}O_{2-\delta}$ is 0.42 S/cm at $p_{O_2} = 5.7 \times 10^{-21}$ atm and 700°C. Thermogravimetric measurements suggests that $\delta = 0.047$ under the same condition, which is equivalent to doping ceria with 22% Sm^{3+}. Therefore, it is estimated that the ionic conductivity under the same condition should be close to *ca*. 0.009 S/cm. Subtraction on the ionic conductivity yields the n-type electronic conductivity of *ca*. 0.41 S/cm. A dilemma for the traditional substituted ceria is that on the one hand the ionic conductivity is increased by orders of magnitude when oxygen vacancies are formed as a consequence of substitution with lower valent cations, on the other hand such substitution generally leads to a considerable decrease in the electronic conductivity. The $(Ce_{0.83}Sm_{0.17})_{0.7}Zr_{0.3}O_{2-\delta}$ solid solution appears to have a relatively good combined electronic and ionic conductivity typically required for solid oxide fuel cell (SOFC) anode materials. Even though the desirable electronic conductivity requirement for anode materials for SOFC (σ_e > 100 S/cm) is not satisfied, $(Ce_{0.83}Sm_{0.17})_{0.7}Zr_{0.3}O_{2-\delta}$ solid solution together with a current collector might be a good choice for the anode material in SOFC.

Table I. Variation of stoichiometry of $Ce^{4+}_{(0.83\times0.7)-2\delta}Ce^{3+}_{2\delta}Sm_{(0.17\times0.7)}Zr_{0.3}O_{1.94-\delta}$ under reducing atmospheres.

Log (p_{O_2}) (atm)	δ	Formula
−17.3	0.0274	$Ce^{4+}_{0.526}Ce^{3+}_{0.0548}Sm_{0.119}Zr_{0.3}O_{1.913}$
−17.9	0.0312	$Ce^{4+}_{0.519}Ce^{3+}_{0.0624}Sm_{0.119}Zr_{0.3}O_{1.909}$
−19.0	0.0372	$Ce^{4+}_{0.507}Ce^{3+}_{0.0744}Sm_{0.119}Zr_{0.3}O_{1.903}$
−19.4	0.0393	$Ce^{4+}_{0.502}Ce^{3+}_{0.0786}Sm_{0.119}Zr_{0.3}O_{1.901}$
−20.1	0.0467	$Ce^{4+}_{0.488}Ce^{3+}_{0.0934}Sm_{0.119}Zr_{0.3}O_{1.893}$
−20.3	0.0494	$Ce^{4+}_{0.482}Ce^{3+}_{0.0988}Sm_{0.119}Zr_{0.3}O_{1.891}$
−21.3	0.0536	$Ce^{4+}_{0.474}Ce^{3+}_{0.107}Sm_{0.119}Zr_{0.3}O_{1.886}$

The increase of electrical conductivity with increased ZrO_2 doping can be attributed to the enhancement of the reducibility of the $(Ce_{0.83}Sm_{0.17})_{1-x}Zr_xO_{2-\delta}$ solid solutions induced by the addition of the Zr into the CeO_2 lattice. According to Balducci *et al.*,[9] the Ce^{4+}/Ce^{3+} reduction energy is significantly reduced even by a small amount of zirconia for CeO_2-ZrO_2 solid solution. In addition, activation-energy calculations indicate an increase of oxygen mobility with increasing zirconia content for CeO_2-ZrO_2 solid solution.[9] The high mobility of oxygen vacancies through the bulk and the surface will assist the Ce^{4+}/Ce^{3+} redox cycle. All these factors will contribute to the enhancement of electronic conductivity.

Ionic and electronic transference numbers.—The Nernst potential and open-circuit voltage of the air-H_2 and air-Ar oxygen concentration cells as a function of temperature are shown in Fig. 9. The bulk and total resistances of the concentration cells were determined from the intercepts of the impedance spectra with the real-axis at high and low frequencies, respectively.

The average oxide ionic transference numbers, t_i, of $(Ce_{0.83}Sm_{0.17})_{0.7}Zr_{0.3}O_2$ were determined from the combination of impedance spectroscopy and open-circuit potential measurement using the equation[24]

$$t_i = 1 - \frac{R_b}{R_t}\left(1 - \frac{V_{oc}}{E_N}\right) \qquad [10]$$

where R_b and R_t are the bulk and total resistance, respectively, of the air-H_2 and air-Ar cells as determined from the impedance-spectroscopy measurement, and V_{oc} and E_N are the open-circuit potential and Nernst potential across the cells, respectively. Furthermore, the average ionic transference numbers, t_i, were calculated from the combination of oxygen permeation and impedance measurements using the following equation[25]

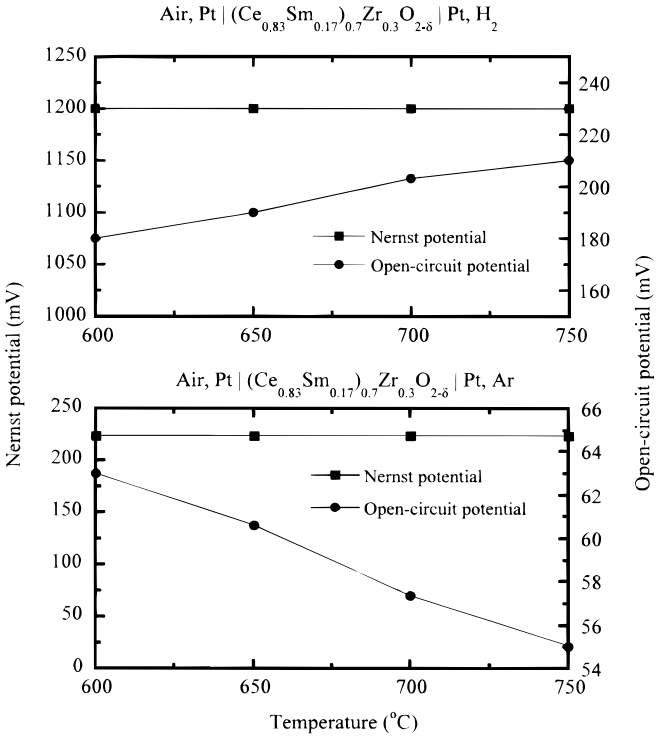

Figure 9. Nernst potential and open-circuit potential of oxygen concentration cell with the configuration of (a, top) air, Pt | $(Ce_{0.83}Sm_{0.17})_{0.7}Zr_{0.3}O_{2-\delta}$ | Pt, H_2 and (b, bottom) air, Pt | $(Ce_{0.83}Sm_{0.17})_{0.7}Zr_{0.3}O_{2-\delta}$ | Pt, Ar measured at different temperatures.

S0013-4651(00)03-078-0 CCC: $7.00

$$t_i = \left(1 - \frac{R_b}{R_t}\right) + \frac{R_b}{\left(\frac{E_N}{I_{O^{2-}}}\right)} \quad [11]$$

The ionic current due to the permeation of oxygen through the oxygen concentration cell, $I_{O^{2-}}$, can be calculated as[26]

$$I_{O^{2-}} = \frac{85.59(V_2X_2 - V_1X_1)}{T} \quad [12]$$

where V_2 and V_1 are the flow rate (mL/min) of the outgoing and incoming gas, respectively, and X_2 and X_1 are the oxygen partial pressures (atm) of the outgoing and incoming gas, respectively. T is the absolute temperature at which the gas flow rate was measured.

The average oxygen ion transference numbers of $(Ce_{0.83}Sm_{0.17})_{0.7}Zr_{0.3}O_{2-\delta}$, as determined from the air-H_2 and air-Ar oxygen concentration cells using Eq. 11 and 12 are shown in Fig. 10. In the air-H_2 cell, the average ionic transference numbers obtained from the combination of gas permeation and impedance spectra are more reliable than those from the combination of open-circuit potential and impedance spectra, since the open-circuit potentials are relatively small. While in the air-Ar cell, the average ionic transference numbers obtained from the combination of gas permeation and impedance spectra and those from the combination of open-circuit potential and impedance spectra agree quite well, it can be seen that in the air-H_2 cell, $(Ce_{0.83}Sm_{0.17})_{0.7}Zr_{0.3}O_{2-\delta}$ exhibits mixed ionic-electronic conduction with mainly electronic conduction in the temperature range of 600 to 750°C. On the other hand, in the air-Ar cell, $(Ce_{0.83}Sm_{0.17})_{0.7}Zr_{0.3}O_{2-\delta}$ shows mixed conduction with predominantly ionic character.

Electrode polarization resistance.—In Fig. 11 and 12 two series of impedance diagrams recorded at higher (650°C) and lower (500°C) temperatures for $(Ce_{0.83}Sm_{0.17})_{0.7}Zr_{0.3}O_{2-\delta}$ are presented. In both cases, the diagrams exhibit two well-defined semicircles representing the properties of the solid electrolyte at higher frequencies and those of the electrodes at low frequencies. The solid-electrolyte

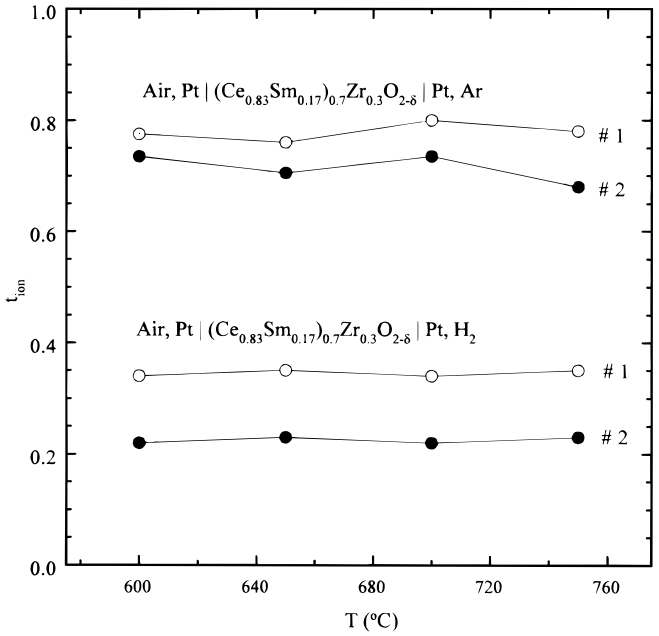

Figure 10. Average oxygen ion transference numbers of $(Ce_{0.83}Sm_{0.17})_{0.7}Zr_{0.3}O_{2-\delta}$ determined at different temperatures using method 1 (Eq. 10) and method 2 (Eq. 11) in a cell of (a) air, Pt | $(Ce_{0.83}Sm_{0.17})_{0.7}Zr_{0.3}O_{2-\delta}$ | Pt, H_2 and (b) air, Pt | $(Ce_{0.83}Sm_{0.17})_{0.7}Zr_{0.3}O_{2-\delta}$ | Pt.

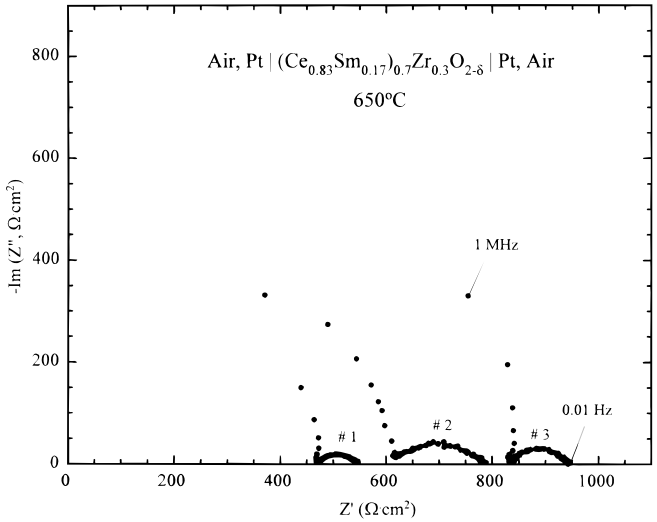

Figure 11. The complex-impedance plots for the cell, air, Pt | $(Ce_{0.83}Sm_{0.17})_{0.7}Zr_{0.3}O_{2-\delta}$ | Pt, air at 650°C (thickness of the three samples: no. 1, 0.96 mm; no. 2, 1.26 mm; no. 3, 1.7 mm).

resistance and the total resistance of the electrochemical cell, Air, Pt | $(Ce_{0.83}Sm_{0.17})_{0.7}Zr_{0.3}O_{2-\delta}$ | Pt, Air were determined from the intercepts of the impedance loops with the real axis at high (*ca.* 0.1 MHz) and low (10^{-3} to 1 Hz) frequencies, respectively. As can be seen in Fig. 11, a wide variation in electrode polarization resistance (5 to 50 Ω-cm^2 at 650°C, as calculated from the three cells consisting of electrolyte materials with different thicknesses in Fig. 11) is observed. The electrode polarization resistances for both the reference electrode and the working electrode are plotted in Fig. 13. The polarization resistances of the electrodes show different slopes indicating different mechanisms of electrode polarizations (in the reference electrode, R1, Pt-mesh collector was incorporated) and increase by four orders of magnitude when the temperature is decreased by 200°C (from 650 to 450°C).

Conclusion

$(Ce_{0.83}Sm_{0.17})_{1-x}Zr_xO_{2-\delta}$ (x = 0 to 0.5) solid solutions were prepared by the hydrothermal method at 260°C. When these samples are calcined at 1500°C, the XRD exhibit a fluorite pattern. The electronic

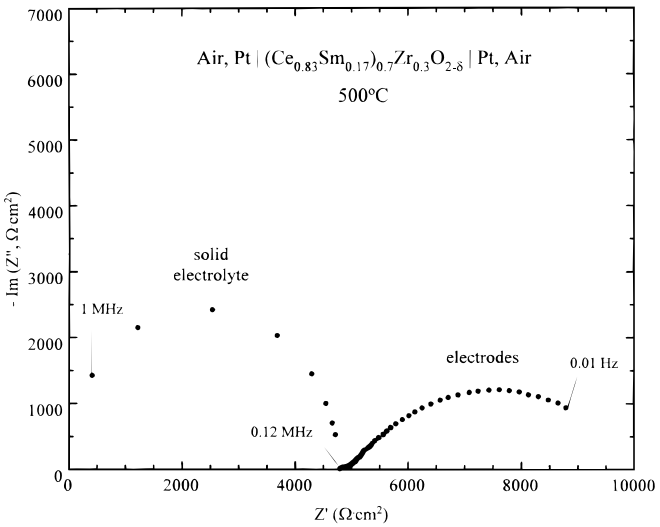

Figure. 12. The complex-impedance plot for the cell, air, Pt | $(Ce_{0.83}Sm_{0.17})_{0.7}Zr_{0.3}O_{2-\delta}$ | Pt, air at 500°C.

S0013-4651(00)03-078-0 CCC: $7.00

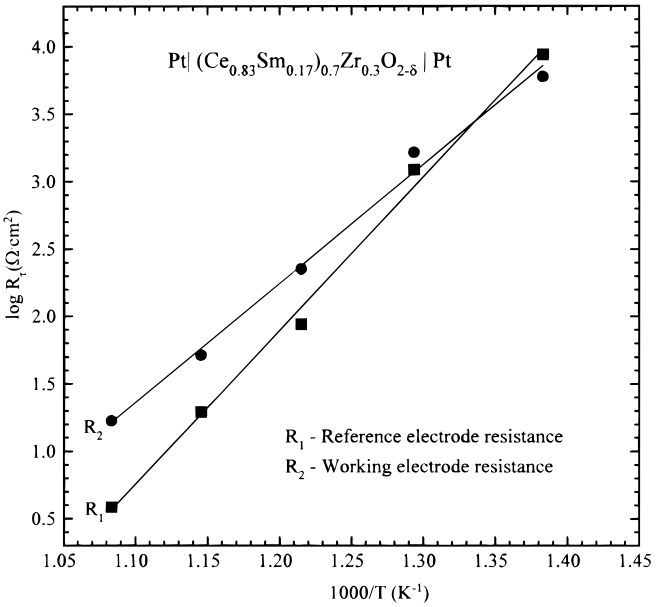

Figure. 13. Temperature dependence of electrode polarization resistance in the cell, air, Pt | $(Ce_{0.83}Sm_{0.17})_{0.7}Zr_{0.3}O_{2-\delta}$ | Pt, air.

conductivity increases dramatically for the $(Ce_{0.83}Sm_{0.17})_{0.7}Zr_{0.3}O_{2-\delta}$ composition in reducing atmospheres. The $(Ce_{0.83}Sm_{0.17})_{0.7}Zr_{0.3}O_{2-\delta}$ solid solution appears to have a relatively good combined electronic and ionic conductivity; the total conductivity is 0.42 S/cm at $p_{O_2} = 5.7 \times 10^{-21}$ atm and 700°C; the ionic conductivity is estimated to be close to *ca*. 10^{-2} S/cm.

References

1. *Application of Solid Electrolytes*, T. Takahashi and A. Kozawa, Editors, JEC Press, Cleveland, OH (1980).
2. *High Conductivity Solid Ionic Conductors*, T. Takahashi, Editor, World Scientific, Singapore (1989).
3. *Chemical and Biochemical Sensors*,Vol. 2,3, W. Göpel, T. A. Jones, M. Kleitz, I. Lundström, and T. Seiyama, Editors, VCH, Weinheim, Germany (1991/1992).
4. H. Inaba and H. Tagawa, *Solid State Ionics*, **83**, 1 (1983).
5. A. Trovarelli, *Catal. Rev.-Sci. Eng.*, **38**, 439 (1996).
6. P. J. Gellings and H. J.-M. Bouwmeester, *Catal. Today*, **1**, 1(1992).
7. P. Shuk, M. Greenblatt, and M. Croft, *Chem. Mater.*, **11**, 273 (1999).
8. P. Shuk and M. Greenblatt, *Solid State Ionics*, **116**, 217 (1999).
9. G. Balducci, J. Kaspar, P. Fornasiero, and M. Graziani, *J. Phys. Chem. B*, **101**, 1750 (1997).
10. G. Balducci, P. Fornasiero, R. Di Monte, J. Kaspar, S. Meriani, and M. Graziani, *Catal. Lett*., **33**, 193 (1995).
11. P. Fornasiero, G. Balducci, D. Di Monte, J. Kaspar, V. Sergo, G. Gubitosa, A. Ferrero, and M. Graziani, *J. Catal.*, **164**, 173 (1996).
12. S. Rossignol, F. Gerard, and D. Duprez, *J. Mater. Chem.*, **9**, 1615 (1999).
13. T. Masui, Y. Peng, K. Machida, and G. Adachi, *Chem. Mater.*, **10**, 4005 (1998).
14. W. Huang, P. Shuk, and M. Greenblatt, *Chem. Mater.*, **9**, 2240 (1997).
15. T. Guo and M. den Boer, *Phys. Rev., B*, **31**, 6233 (1984).
16. *X-Ray Absorption: Principles, Applications, Techniques of EXAFS SEXAFS, and XANES*, D. Koningsberger and R. Rrins, Editors, John Wiley & Sons, Inc., New York (1988).
17. M. Croft, D. Sills, M. Greenblatt, C. Lee, S-W. Cheong, K. V. Ramanujachary, and D. Tran, *Phys. Rev., B*, **55**, 8726 (1997).
18. V. Agarwal and M. Liu, *J. Electrochem. Soc.*, **144**, 1035 (1997).
19. B. Cales and J. F. Baumard, *J. Electrochem. Soc.*, **131**, 2407 (1984).
20. R. D. Shannon, *Acta Crystallogr., Sect. A*, **32**, 751 (1976).
21. R. Orlando, C. Pisani, C. Roetti, and E. Stefanovich, *Phys. Rev. B*, **45**, 592 (1992).
22. F. A. Kröger, *The Chemistry of Imperfect Crystals*, Vol. 2, p. 40, American Elsevier Pub. Corp., New York (1974).
23. M. Mogensen, T. Lindegaard, and U. R. Hansen, *J. Electrochem. Soc.*, **141**, 2122 (1994).
24. M. Liu and H. Hu, *J. Electrochem. Soc.*, **143**, L109 (1996).
25. F. Chen and M. Liu, *J. Solid State Electrochem.*, **3**, 7 (1998).
26. M. Liu and A. Joshi, in *Proceedings of the First International Symposium on Ionic and Mixed Conducting Ceramics*, T. A. Ramanarayanan and H. L. Tuller, Editors, PV 91-12, p. 231, The Electrochemical Society Proceedings Series, Pennington, NJ (1991).